Research Square

Preprints are preliminary reports that have not undergone peer review.
They should not be considered conclusive, used to inform clinical practice,
or referenced by the media as validated information.

Dynamic Light Regulation of Surface CO Coverage Enables Efficient Low-Temperature RWGS on Electron-Rich Pt

Zhaoke Zheng

zkzheng@sdu.edu.cn

Shandong University https://orcid.org/0000-0003-1104-2583

Guo Qingzheng

Shandong university https://orcid.org/0009-0007-7698-1350

Haopeng Ge

Shandong University

Guangyao Zhai

Shandong Normal University

Zeyan Wang

Shandong University https://orcid.org/0000-0002-0723-4956

Yuanyuan Liu

Shandong University

Peng Wang

State Key Laboratory of Crystal Materials https://orcid.org/0000-0003-4250-8104

Hefeng Cheng

Shandong University https://orcid.org/0000-0002-9135-8109

Ying Dai

Shandong University

Baibiao Huang

Shandong University

Article

Keywords: surface adsorbate regulation, RWGS, photo-assisted thermal catalysis, CO poisoning mitigation

Posted Date: August 5th, 2026

DOI: https://doi.org/10.21203/rs.3.rs-10531358/v1

License: This work is licensed under a Creative Commons Attribution 4.0 International License.
Read Full License

Additional Declarations: There is **NO** Competing Interest.

Abstract

Surface poisoning by strongly adsorbed intermediates severely limits the efficiency of heterogeneous catalysts, yet dynamically regulating adsorbate coverage under reaction conditions remains highly challenging. Here we report that light irradiation can dynamically regulate CO surface coverage on electron-rich Pt-MoO_{3-x} catalysts and thereby promote the reverse water–gas shift (RWGS) reaction under low-temperature conditions. Consequently, the Pt-MoO_{3-x} catalyst exhibits markedly enhanced catalytic activity under full-spectrum illumination compared with dark conditions at identical catalyst temperatures. In situ XPS measurements reveal illumination-induced electron enrichment of Pt sites, indicating interfacial charge redistribution across the Pt–O–Mo interface. The continuous-flow CO-DRIFTS experiments simulate a CO-supplemented environment relevant to RWGS catalysis, revealing a pronounced illumination-induced decrease in the steady-state surface CO coverage, thereby dynamically maintaining the availability of active sites in a product-rich environment. Complementary adsorption–purge DRIFTS experiments further confirm the regulatory effect of light irradiation on chemisorbed CO species. Theoretical calculations bridge these findings and indicate that this robust electron-rich state reshapes the Pt–CO electronic interaction, fundamentally weakening the adsorption and alleviating CO poisoning. This effect cannot be attributed solely to photothermal heating. This work establishes light-mediated dynamic regulation of surface adsorbate coverage as an effective strategy for mitigating catalyst poisoning and enhancing heterogeneous catalytic reactions.

1 Introduction

Controlling the adsorption and desorption of surface intermediates is central to heterogeneous catalysis because excessive adsorption can block active sites and suppress catalytic activity[1]. A representative example is the reverse water–gas shift (RWGS) reaction, which converts CO_2 into CO, providing a key feedstock for downstream chemical synthesis and sustainable carbon utilization[2]. Despite its significance, the RWGS reaction is frequently constrained by the strong adsorption and accumulation of CO-related intermediates, which block active sites, impede reactant activation, and thereby suppress catalytic performance.[3]. Moreover, owing to its endothermic thermodynamic nature[4], the RWGS reaction generally requires elevated operating temperatures, resulting in substantial energy consumption. Therefore, it is highly desirable to develop effective strategies that can dynamically regulate surface adsorbate coverage under milder reaction conditions to achieve efficient CO_2 conversion while mitigating CO accumulation.

Among various RWGS catalysts, Pt-based systems have been widely investigated owing to their excellent capability for H_2 dissociation and activation[5]. However, the intrinsic strong affinity between Pt and CO frequently leads to severe surface poisoning. This behavior originates from the synergistic σ-donation and π-back-donation interactions between Pt and CO, which stabilize adsorbed CO and hinder the availability of Pt sites for subsequent reactant activation[1a, 6]. To alleviate CO poisoning, various strategies have been explored, including tuning metal–support interactions[7], improving metal

dispersion such as constructing single-atom catalysts[8], and engineering interfacial structures[9]. Although these approaches can improve CO tolerance to some extent, they primarily rely on static structural modifications. Because CO is continuously generated and replenished at the catalyst surface during the RWGS reaction, static catalyst structures are generally incapable of dynamically balancing CO accumulation and removal, leading to progressive site blocking and performance loss. These challenges underscore the critical importance of developing strategies capable of dynamically regulating steady-state CO coverage under reaction conditions, thereby overcoming the inherent limitations of static catalyst design.

In this context, light irradiation emerges as an ideal external stimulus, providing unique opportunities to regulate catalytic pathways through mechanisms fundamentally distinct from conventional thermocatalysis[10]. In addition to photothermal effects, light can modify charge distribution and electronic structures at catalyst interfaces, thereby altering the adsorption and activation behavior of surface intermediates[11]. This offers a powerful means to actively manipulate the electronic states of metal active sites under operando conditions. Given that the binding affinity of strongly adsorbed species such as CO is highly sensitive to the local electronic environment of metal surfaces[12], illumination-induced regulation of the catalyst electronic structure may provide an effective strategy for dynamically controlling steady-state CO coverage under reaction conditions. However, the application of such concepts to mitigate CO poisoning during heterogeneous catalysis remains largely unexplored.

Herein, we report a Pt-MoO_{3-x} catalyst that enables light-mediated regulation of surface CO coverage during the RWGS reaction (Fig. 1). Benefiting from this unique regulatory mechanism, the catalyst exhibits exceptional performance under full-spectrum illumination (2.8 W cm^{-2}), achieving a remarkable CO yield of 1246 mmol g_{cat}^{-1} h^{-1} with over 99% selectivity. In situ XPS measurements reveal illumination-induced electron enrichment of Pt sites, indicating interfacial charge redistribution across the Pt–O–Mo interface. Correspondingly, continuous-flow CO-DRIFTS experiments performed under a CO-supplemented environment relevant to RWGS catalysis demonstrate a pronounced illumination-induced decrease in steady-state CO coverage. Complementary adsorption–purge DRIFTS measurements further confirm the light-mediated regulation of chemisorbed CO species. Theoretical calculations further reveal that electron-rich Pt sites weaken Pt–CO interactions and facilitate CO removal, providing an electronic-structure basis for the experimentally observed modulation of surface CO coverage. Crucially, rigorous temperature monitoring using both infrared thermography and a direct-contact thermocouple unequivocally decouples the observed catalytic enhancement from conventional photothermal heating. This work highlights light-mediated regulation of surface adsorbates as a promising strategy for mitigating catalyst poisoning and tuning heterogeneous catalytic reactions.

2. Results and Discussion

2.1Catalytic performance for RWGS reaction

Under full-spectrum illumination (2.8 W cm^{-2}, 350–1200 nm) without external heating, the catalyst temperature reached approximately 350°C, as measured by both infrared thermometry and an internal thermocouple (Figure S1 and S2). To ensure accurate temperature determination, the reactor was equipped with an infrared-transparent KBr window instead of a conventional quartz window, thereby minimizing interference with infrared temperature measurements. In addition, the internal thermocouple was positioned to maximize contact with the catalyst bed, ensuring reliable monitoring of the actual catalyst temperature. Under these conditions, the Pt-MoO_{3-x} catalyst exhibited a maximum CO production rate of 1246 mmol g_{cat}^{-1} h^{-1} with a selectivity higher than 99.9% (Figure S5). The catalytic performance compares favorably with representative RWGS catalysts reported under comparable reaction conditions (Fig. 2c). Notably, the catalytic activity under light irradiation was nearly three times higher than that obtained under purely thermal conditions at an identical catalyst temperature of 350°C (Figs. 2a, S5 and S6). In contrast, MoO_{3-x} without Pt produced only 0.06 mmol g_{cat}^{-1} h^{-1} of CO under identical illumination conditions (Figure S7), indicating that Pt sites are essential for the RWGS reaction.

Moreover, Pt-MoO_{3-x} maintained highly stable CO selectivity during a 200 hours continuous test (Fig. 2b). Post-reaction characterization showed that the catalyst framework remained largely preserved after catalysis: XRD and Raman spectra exhibited no discernible phase or structural changes (Figure S8b and S9), whereas STEM analysis revealed a modest increase in the average Pt particle size from ~ 2.3 nm to ~ 3.0 nm (Figure S10). X-ray photoelectron spectroscopy (XPS) analysis (Figure S11) showed that the surface Mo species underwent slight reoxidation during the RWGS reaction, whereas the characteristic electronic state of Pt was largely preserved. In addition, the O 1s spectrum of the spent catalyst exhibited a new high-binding-energy component (~ 533 eV), which can be assigned to adsorbed H_2O/hydroxyl species generated during the RWGS reaction. Importantly, the O 1s component associated with oxygen vacancies remained clearly detectable after the reaction, indicating that oxygen vacancies were largely retained during long-term operation. These results suggest that although minor surface and nanoparticle evolution occurs during prolonged operation, Pt-MoO_{3-x} retains its overall structural integrity under photothermal RWGS conditions.

To further examine the structural implications of reaction temperature, the catalyst was additionally evaluated under conventional high-temperature RWGS conditions. When Pt-MoO_{3-x} was tested at 700°C, pronounced aggregation of Pt nanoparticles was observed after 8 h of reaction, accompanied by a substantial decline in catalytic performance (Figures S12 and S13). In contrast to the relatively minor structural evolution observed under illumination-assisted operation at 350°C, the catalyst underwent much more severe morphological changes at elevated temperatures, indicating accelerated Pt sintering and loss of accessible active sites under conventional thermal RWGS conditions. These observations suggest that low-temperature operation is advantageous for preserving Pt dispersion and structural integrity during RWGS catalysis.

The catalytic activity was found to increase with increasing light intensity (Figures S14 and S15). When the light intensity was increased to 4.0 W cm^{-2}, the catalyst temperature reached approximately 390°C

and the CO production rate increased to 2548 mmol g_{cat}^{-1} h^{-1} (Figure S16 and S17), indicating a pronounced dependence of catalytic performance on illumination conditions. The pronounced activity enhancement under illumination at identical temperatures suggests that factors beyond purely photothermal heating contribute to the catalytic behavior of Pt-MoO_{3-x}. The influence of reaction parameters on catalytic performance was also examined. As shown in Figure S18, increasing the GHSV led to a progressive increase in the CO production rate, reaching the highest value at 360 L g_{cat}^{-1} h^{-1}. In addition, the CO production rate increased with increasing H_2 fraction, and the optimal activity was obtained at a CO_2/H_2 ratio of 1:1 (Figure S19). The dependence of catalytic activity on the CO_2/H_2 ratio suggests the existence of an optimal reactant balance. The superior performance at CO_2/H_2 = 1:1 may arise from a balanced interplay between CO_2 activation on oxygen-deficient MoO_{3-x} sites and H_2 activation on Pt. Excessive H_2 concentrations may alter surface coverage or competitive adsorption behavior, leading to no further improvement in activity.

The influence of Pt loading on catalytic activity was further investigated. As shown in Figure S6, increasing the Pt loading gradually enhanced the catalytic performance. However, when the Pt loading reached 1.8 wt%, the CO_2 conversion no longer increased significantly. Therefore, catalysts containing 1.8 wt% Pt were used for subsequent studies unless otherwise specified.

To further understand the role of the support, different oxide supports were evaluated under identical reaction conditions (2.8 W cm^{-2} illumination). As shown in Fig. 2e, the CO production rate of $Pt_{1.8}$-TiO_2 was 310 mmol g_{cat}^{-1} h^{-1}, which is significantly lower than that of $Pt_{1.8}$-MoO_{3-x}. Meanwhile, $Pt_{1.8}$-Al_2O_3 exhibited negligible catalytic activity under identical conditions, likely reflecting the limited CO_2 activation capability of Al_2O_3[5d, 13]. Interestingly, when fully oxidized pristine MoO_3 was used as the support, the catalyst initially exhibited a relatively low CO production rate of 350 mmol g_{cat}^{-1} h^{-1} (Figure S20). However, the activity gradually increased during the reaction and reached 1207 mmol g_{cat}^{-1} h^{-1} after 6.5 h. Post-reaction XPS analysis (Figure S21b) revealed the formation of abundant oxygen vacancies on the catalyst surface, indicating that the catalyst can undergo self-reduction under the reaction atmosphere[14]. The concomitant evolution of catalytic activity and oxygen-vacancy formation highlights the important role of oxygen-deficient MoO_{3-x} environments in promoting RWGS catalysis. These observations further indicate that such oxygen-deficient environments are closely associated with the unique Pt interfacial properties and light response of the Pt-MoO_{3-x} catalyst.

2.2 Characterization and structure analysis of Pt-MoO_{3-x}

We synthesized oxygen-deficient MoO_{3-x} using a simple hydrothermal method[15]. X-ray photoelectron spectroscopy (XPS) analysis (Figure S21a) revealed mixed-valence Mo species (Mo^{6+}/Mo^{5+}), consistent with the formation of oxygen-deficient MoO_{3-x}. Using chloroplatinic acid as the Pt source, a series of Pt-loaded MoO_{3-x} catalysts with different Pt loadings were prepared via an ice-template method[16], and the

resulting catalysts are denoted as Pt-MoO_{3-x}. Synthesis route is shown in Figure S22. The oxygen-deficient nature of MoO_{3-x} is proposed to facilitate the anchoring and dispersion of fine Pt nanoparticles during the reduction process associated with the ice-template synthesis. Pd-MoO_{3-x}, Pt-Al_2O_3, and Pt-TiO_2 were also prepared using the same method (Figure S23). High-resolution transmission electron microscopy (HRTEM) and energy-dispersive X-ray spectroscopy (EDS) showed that Pt nanoparticles were uniformly distributed on the surface of well-shaped MoO_{3-x} nanosheets, with average particle size of ~ 2.3 nm (Figures S9a and S24). As shown by the XRD patterns (Figure S25), no obvious changes in the diffraction features of MoO_{3-x} are observed before and after Pt loading, indicating that the crystal structure of MoO_{3-x} is well preserved. The lattice spacing of 0.23 nm can be assigned to the (111) plane of Pt, and that of 0.28 nm corresponds to the (101) plane of MoO_{3-x} (Fig. 3a). XPS and electron paramagnetic resonance (EPR) analyses (Fig. 3d, Figure S26 and Figure S27) indicated that Pt-MoO_{3-x} possesses a higher concentration of oxygen vacancies than bare MoO_{3-x}.

To elucidate electronic interactions at the Pt-MoO_{3-x} interface, in situ XPS measurements were performed under dark and illumination conditions (Fig. 3b,3c and S27). Positive binding-energy shifts were observed for Mo 3d (0.36 eV) and O 1s (1.22 eV), accompanied by a negative shift in Pt 4f (0.32 eV), indicating electron depletion within the MoO_{3-x} support and concurrent electron enrichment at Pt sites under illumination. The comparatively larger shift of O 1s suggests a prominent involvement of interfacial oxygen species in the charge redistribution process, consistent with a Pt–O–Mo interfacial environment. The resulting illumination-induced electron enrichment of Pt is expected to modify Pt–CO interactions and thereby influence the evolution of surface CO coverage under reaction conditions.

In H_2-TPD experiments (Figure S28), Pt-MoO_{3-x} displays a prominent desorption peak at approximately 200°C, significantly lower than the ~ 400°C peak observed for bare MoO_{3-x}. This behavior indicates enhanced H_2 activation and increased hydrogen mobility upon Pt incorporation. Pt sites facilitate dissociative H_2 adsorption, generating reactive atomic hydrogen (H*) that can migrate to the MoO_{3-x} support through hydrogen spillover. This shift reflects the exceptional capability of Pt to provide low-energy pathways for the dissociative chemisorption of H_2. H_2-TPR measurements (Figure S29) demonstrate a substantial reduction peak at ~ 330°C for Pt-MoO_{3-x}, nearly 200°C lower than the ~ 520°C peak for unsupported MoO_{3-x}. This pronounced shift highlights the strong promotional effect of Pt on the reducibility of the oxide support. The dissociative activation of H_2 on Pt generates mobile hydrogen species that readily migrate across the Pt–MoO_{3-x} interface, thereby facilitating the reduction of Mo species at substantially lower temperatures.

As illustrated in Figure S31, The incorporation of Pt greatly enhanced the thermal stability of MoO_{3-x}. MoO_{3-x} rapidly decomposed above 700°C, losing more than 43% of its weight at 1000°C. In comparison, the Pt-MoO_{3-x} catalyst only lost 15% of its weight even under high-temperature conditions at 1100°C. The improved thermal robustness is likely associated with strong Pt-support interactions and the modified electronic/defect environment introduced by Pt incorporation, which help stabilize the oxygen-

deficient oxide framework at elevated temperatures. Combined with the post-reaction XRD, Raman, STEM, and XPS analyses discussed above, these observations indicate that Pt-MoO_{3-x} retains substantial structural integrity despite minor nanoparticle growth and surface evolution during prolonged RWGS operation.

The effective utilization of light and the photothermal conversion performance of the catalysts were systematically investigated. As shown by photoluminescence spectroscopy (Fig. 3e), Pt-MoO_{3-x} exhibits significantly lower PL intensity than pristine MoO_{3-x}, indicating altered excited-state relaxation behavior after Pt incorporation. The reduced PL emission is consistent with enhanced non-radiative energy dissipation pathways, which may contribute to improved photothermal conversion performance. In addition, UV–Vis–NIR absorption spectroscopy (Figure S32) reveals that Pt-MoO_{3-x} exhibits strong broadband light absorption across the 200–1000 nm range. This broad absorption can be associated with oxygen-vacancy-related electronic transitions and LSPR-like behavior in oxygen-deficient MoO_{3-x}[5, 15], thereby facilitating effective light harvesting. Consistent with these optical characteristics, the catalyst displays excellent photothermal conversion capability: without external heating, the catalyst surface temperature rapidly exceeds 350°C under full-spectrum illumination at 2.8 W cm^{-2}, and surpasses 400°C at 4.0 W cm^{-2} (Figures S17). Crucially, this robust photothermal effect provides the necessary thermal baseline to drive the endothermic RWGS reaction.

2.3 Measurement and discussion of CO desorption

An increase of apparent activation energy is commonly observed when the catalyst undergoes poisoning, deactivation, or surface reconstruction, which leads to deterioration in its intrinsic catalytic performance[17]. At the same temperature, the apparent activation energy of Pt-MoO_{3-x} under thermocatalytic (dark) conditions was calculated to be 45.5 ± 0.2 kJ mol^{-1}, whereas under photothermal (light) conditions it decreased to 34.3 ± 0.1 kJ mol^{-1} (Fig. 2d). This substantial reduction suggests that light irradiation facilitates the RWGS reaction through a mechanism beyond conventional thermal activation.

Because CO accumulation is widely recognized as a major factor limiting Pt-catalyzed RWGS reactions, we hypothesized that this lowered activation energy originates from the light-mediated mitigation of CO poisoning. To rigorously test this, in situ diffuse reflectance infrared Fourier transform spectroscopy (DRIFTS) was employed. Specifically, continuous-flow CO-DRIFTS experiments were conducted under a steady feed of 10% CO/Ar. This design was intended to deliberately establish a continuously replenished CO environment with a high local CO concentration, thereby mimicking the sustained accumulation of CO that may occur during the RWGS reaction. Such conditions provide a stringent platform for evaluating whether illumination can effectively regulate steady-state CO coverage on Pt sites.

Catalyst temperature was monitored using an embedded thermocouple positioned directly within the catalyst bed, and light/dark experiments were compared at identical catalyst temperatures to minimize ambiguity arising from photothermal heating (Figure S33). Under these high-coverage conditions, the

analysis focused on the CO stretching vibration region. The peak area of the CO stretching vibration region at 25°C was defined as A_0, representing the maximum CO coverage in the dark. The peak areas (A) at various temperatures were normalized by A_0 to calculate the relative surface CO coverage (A/A_0).

As shown in Figs. 4a, S34 and S35, increasing temperature gradually decreased the steady-state CO signal intensity under dark conditions. Notably, under illumination at the same catalyst temperature, a more pronounced decrease in the CO-related infrared intensity was observed. At 420°C, the normalized CO signal decreased by ~ 36% in the dark but by ~ 50% under illumination. These results indicate that light illumination lowers steady-state CO surface populations under continuous CO supply conditions, consistent with mitigation of CO poisoning during RWGS catalysis.

Because no measurable illumination-induced change in the CO-related infrared response was observed for bare MoO_{3-x} (Figure S36), the modulation of CO behavior under illumination cannot originate solely from the oxide support and instead requires the presence of metal sites. This observation is consistent with the negligible RWGS activity of MoO_{3-x} under identical reaction conditions and highlights the essential role of Pt in governing surface CO evolution.

Additional catalytic evidence supporting light regulated CO behavior was obtained from low-temperature RWGS experiments (Figs. 4c and 4d). Under illumination, Pt-MoO_{3-x} already exhibited 54% CO selectivity at a catalyst temperature of 50°C, which further increased to 82% at 100°C. By contrast, under dark conditions, Pt-MoO_{3-x} showed only 13.6% CO selectivity at 100°C, while CH_4 became the dominant product (86.4%). The markedly different product distributions suggest that illumination substantially alters the fate of surface carbon-containing intermediates on Pt surfaces. In the absence of illumination, retained CO species are more prone to further hydrogenation, whereas illumination favors higher steady-state CO release and suppresses over-hydrogenation pathways. This interpretation is fully consistent with the continuous-flow CO-DRIFTS results, which reveal a significantly lower steady-state CO coverage under illuminated conditions.

To further examine the wavelength dependence of light regulated CO behavior, band-selective illumination experiments were performed (Figs. 4e and S37). Under identical light intensities, Pt-MoO_{3-x} exhibited the most pronounced reduction in steady-state CO surface coverage under 450 nm irradiation. Specifically, the temperatures required to decrease the normalized CO signal to 90%, 80%, and 70% were 57°C, 166°C, and 301°C, respectively, which are substantially lower than those obtained under 350 nm or 650 nm illumination. This wavelength-dependent behavior is consistent with the optical characteristics of Pt-MoO_{3-x} and further supports that illumination-induced regulation of surface CO coverage depends on photon energy rather than arising solely from thermal effects.

To verify whether this illumination-responsive is unique to Pt, Pd-MoO_{3-x} was evaluated under identical RWGS conditions as a control (Fig. 4f). In sharp contrast to the Pt system, Pd-MoO_{3-x} displayed no significant activity enhancement or selectivity variations under illumination (Figure S38), indicating that light irradiation fails to induce measurable changes in catalytic behavior. Interestingly, the Pd catalyst

sustained slightly higher surface temperatures under illumination (Figure S39). The higher catalyst temperature observed suggests that absorbed photon energy is more efficiently dissipated as heat rather than contributing to illumination-responsive modulation of surface CO behavior. In situ continuous-flow CO-DRIFTS measurements on Pd-Al_2O_3 further corroborate this metal-dependent behavior under reaction-relevant environments (Figure S40). Under a continuous CO atmosphere, Pd-Al_2O_3 exhibited negligible spectral differences between the illuminated and dark conditions, showing none of the pronounced steady-state CO coverage suppression characteristic of the Pt system. These comparative results unambiguously demonstrate that the light-mediated dynamic regulation of adsorbate coverage is not a universal trait among platinum-group metals, but is strictly dictated by the unique electronic structure of the metal center, highlighting a strong metal-dependent behavior in illumination -induced CO regulation.

To further distinguish illumination-induced changes in adsorbed CO species from possible gas-phase contributions, complementary adsorption–purge DRIFTS experiments were subsequently performed. After CO saturation, the catalyst was extensively purged with Ar prior to spectral acquisition and illumination treatment, thereby minimizing contributions from gas-phase CO (Fig. 4b). Under these strictly purged conditions, the residual CO-related features smoothly isolated into the spectral range characteristic of solely chemisorbed CO on Pt sites. The residual *v*CO region consisted of two major absorption features located at ca. 2000–2100 cm^{-1} and 1700–1900 cm^{-1}. These spectral regions are generally associated with linearly adsorbed CO and bridged/multicoordinated CO species on Pt surfaces, respectively[18]. It should be noted that each spectral region may contain contributions from multiple adsorption environments present on Pt nanoparticles.

Importantly, Pt-MoO_{3-x} still exhibited a pronounced illumination-dependent evolution of the adsorbed CO population under these rigorously purged conditions. Compared with the dark condition, illumination resulted in a more rapid decrease of the residual chemisorbed CO species, demonstrating that the illumination response observed in the continuous-flow experiments is not an artifact arising from gas-phase CO. These adsorption–purge DRIFTS measurements therefore provide independent evidence that illumination influences the behavior of chemisorbed CO species on Pt surfaces.

We recognize that, from the perspective of fundamental surface science, light irradiation may in principle induce spectral shifts through mechanisms such as modified dipole–dipole coupling or Stark effects, potentially leading to misinterpretation of changes in CO peak intensities or areas[19]. However, no such spectral shifts were observed in our experiments. This is likely because the steady-state population of vibrationally excited CO molecules is extremely small under the relatively moderate illumination conditions employed here[11c]. Consequently, these transient species are expected to be below the detection limit of conventional time-averaged FTIR measurements and therefore do not make a measurable contribution to the recorded spectra.

Interestingly, upon increasing temperature under both illuminated and dark conditions, the bridged CO band decreased more rapidly than the linear CO band and eventually became nearly undetectable,

whereas a fraction of linearly adsorbed CO remained on the Pt surface. This observation indicates that different adsorbed CO species exhibit distinct thermal stabilities and desorption behaviors on Pt sites[18b]. The microscopic origin of this behavior remains unclear from spectroscopic observations alone and therefore warrants further electronic-structure analysis.

To further evaluate the generality of this phenomenon, Pt-Al_2O_3 was examined using the same adsorption–purge protocol (Figures S41 and S42). Similar illumination-responsive behavior of adsorbed CO species was observed on both Pt-containing catalysts after removal of gas-phase CO, highlighting the essential role of Pt sites in governing light-mediated CO evolution. Nevertheless, considering the substantially different RWGS activities of Pt-MoO_{3-x} and Pt-Al_2O_3, illumination-responsive CO regulation alone is insufficient to account for catalytic performance and must operate cooperatively with the oxygen-deficient MoO_{3-x} reaction environment.

Taken together, the continuous-flow DRIFTS and adsorption–purge DRIFTS experiments provide complementary lines of evidence. The former captures the dynamic evolution of CO surface coverage under reaction-relevant conditions, whereas the latter directly demonstrates that light irradiation facilitates the removal of chemisorbed CO species, The consistency between these independent observations establishes a robust experimental foundation for understanding how illumination influences Pt–CO interactions.

To fundamentally decode the microscopic physical origins behind the illumination-regulated CO desorption and the distinct thermal stabilities of surface intermediates observed in our in situ DRIFTS measurements, comprehensive density functional theory (DFT) calculations were performed. To isolate the influence of the Pt electronic structure on the Pt–CO interaction, a simplified Pt_4 cluster model was employed in this section. In situ XPS measurements indicate that the primary electronic effect under illumination is electron enrichment at Pt sites. To capture this electronic effect within a ground-state DFT framework, we modulated the interfacial charge transfer through the defect chemistry of the support and examined how variations in the electron density of Pt influence CO adsorption. Specifically, a Pt_4 cluster supported on an oxygen-deficient MoO_{3-x} (010) surface was adopted as the electron-enriched model. In this configuration, oxygen vacancies act as electron donors, increasing the electron density of the supported Pt_4 cluster and thereby providing a representative model for an electron-rich Pt state. For comparison, a Pt_4 cluster supported on pristine MoO_3(010) was employed as the electron-deficient reference model. As visualized by the charge density difference (CDD) and Bader charge analysis (Fig. 5a), the Pt_4 cluster on pristine MoO_3 exhibits an overall electron loss of 0.40 e, whereas the Pt_4 cluster on oxygen-deficient MoO_{3-x} gains 0.61 e. These two models therefore provide a suitable platform for evaluating how changes in Pt electron density influence CO adsorption behavior.

CO adsorption was subsequently investigated on both models using the two adsorption configurations experimentally observed on Pt surfaces, namely linear and bridge adsorption (Figure S43). As depicted in Fig. 5b, the electron-rich Pt sites fundamentally weaken the thermodynamic binding strength of CO.

Specifically, the adsorption energy for the atop configuration decreases from − 2.53 eV on the electron-deficient model to − 2.11 eV on the electron-rich model. An analogous destabilization is observed for the bridged configuration (from − 2.03 eV to − 1.83 eV). Notably, in both models, bridge-bonded CO exhibits intrinsically weaker adsorption than linearly adsorbed CO, which is consistent with our spectroscopic observation that bridged species undergo more rapid thermal desorption prior to the linear species.

To precisely elucidate the orbital-level mechanism driving this weakened interaction, we analyzed the projected density of states (PDOS) focusing on the most persistent linear adsorption configuration (Fig. 5c and 5d). Significant overlap between Pt d states and CO-derived C p states is observed in both models, confirming the formation of Pt–CO bonding interactions. Enlarged PDOS plots near the Fermi level (Fig. 5d) reveal that the CO-derived C p states shift toward lower energies and become more closely aligned with the Pt d states in the electron-rich model. Similar electronic features are also observed for bridge-bonded CO species (Figure S44), suggesting that electron enrichment modifies the Pt–CO interaction irrespective of the adsorption geometry.

To further quantify the strength of the Pt–CO interaction, crystal orbital Hamilton population (COHP) analyses were conducted. For linearly adsorbed CO, the ICOHP value decreases markedly from − 4.94 eV on electron-deficient model to − 2.42 eV on electron-rich model (Fig. 5e), indicating a substantial weakening of the Pt–CO bond upon electron enrichment. This trend is fully consistent with the reduced adsorption energies and supports the experimentally observed decrease in steady-state CO coverage under illumination. Furthermore, COHP analyses of the bridged configurations (Table S5) reveal larger absolute ΣICOHP values than those of the corresponding linear configurations. This behavior originates from the simultaneous interaction of the carbon atom with two Pt atoms, giving rise to two Pt–C bonding contributions. Therefore, ΣICOHP reflects the cumulative strength of multiple Pt–C interactions rather than the strength of an individual Pt–C bond. Although bridged configurations exhibit a larger absolute ICOHP value due to the contribution of two Pt–C bonds, the adsorption energy reflects the overall thermodynamic stability of the adsorbate, which is also influenced by geometric strain and electron redistribution at the interface. As a result, stronger cumulative covalent interaction does not necessarily translate into higher adsorption stability or lower desorption propensity. Indeed, adsorption-energy calculations indicate that bridge adsorption is thermodynamically less stable than linear adsorption on both models, consistent with the experimentally observed preferential disappearance of bridge-bonded CO species during DRIFTS measurements.

Taken together, the DFT results establish a clear correlation between Pt electron enrichment and weakened Pt–CO interactions. Combined with the in situ XPS and DRIFTS measurements, these findings provide a mechanistic explanation for the illumination-induced reduction of steady-state CO coverage and the enhanced RWGS performance observed under illumination.

2.4 Reaction mechanism

To gain mechanistic insight into the RWGS reaction over Pt-MoO_{3-x}, we firstly elucidated the dominant RWGS reaction pathway. In general, the RWGS reaction proceeds via either a redox mechanism or an associative mechanism[20]. Catalysts operating through a redox pathway are capable of generating CO from CO_2 in the absence of H_2, whereas associative pathways typically require the participation of hydrogen-containing surface intermediates[21]. To distinguish between these possibilities, transient sequential in situ DRIFTS measurements (Ar → CO_2 → Ar → H_2) were conducted. As shown in Figure S45 a distinct CO signal was detected on the sample surface after introducing CO_2. Upon subsequent Ar purging and the sequential introduction of H_2, a concomitant signal corresponding to H_2O emerged. These observations indicate that CO_2 can undergo direct dissociation on the oxygen-deficient Pt-MoO_{3-x} surface, producing CO prior to hydrogen participation, which is consistent with a redox-type RWGS pathway (Fig. 6c).

Kinetic isotope effect (KIE) experiments were further performed to probe the influence of hydrogen and carbon dioxide activation on the reaction kinetics (Fig. 6a and S46). In the isotope labeling experiment by substituting D_2 for H_2, the calculated KIE value for Pt-MoO_{3-x} under thermal catalytic conditions was 1.73, while under photothermal catalytic conditions it was as high as 2.19. Under both photothermal and thermal catalytic conditions, the CO generation rate using H_2 as the feed gas was higher than using D_2, this was due to the easier dissociation and faster migration of hydrogen species compared to deuterium[22]. In contrast, when $C^{16}O_2$ was replaced with $C^{18}O_2$, the corresponding KIE values were close to unity (1.07 and 1.06 under thermocatalytic and photothermal conditions, respectively). These starkly contrasting KIE results unequivocally establish that hydrogen activation and migration—rather than CO_2 dissociation—are the kinetically relevant steps in this RWGS process. This perfectly corroborates the proposed redox mechanism: CO_2 rapidly and directly dissociates into gaseous CO on the oxygen-deficient MoO_{3-x} surface, followed by the reduction of the oxidized oxide by hydrogen species. In addition, the loading of Pt also greatly promotes the self-reduction capability of MoO_{3-x} in the RWGS reaction as confirmed by the gradual increase in CO production rate for Pt-MoO_3 (Figure S20). Consequently, the cooperative interplay between oxygen-vacancy-rich MoO_{3-x} and Pt–facilitated hydrogen activation underpins the exceptional catalytic activity of the Pt-MoO_{3-x} catalyst.

Having established that illumination decreases the steady-state CO surface coverage on Pt-MoO_{3-x}, we next employed DFT calculations to evaluate how variations in CO coverage influence the RWGS reaction energetics. A Pt_4 cluster model was used for electronic-structure-sensitive analyses, whereas a larger Pt_{10} cluster was adopted for reaction energetics and multi-adsorbate configurations to better represent coverage effects under realistic reaction conditions. In particular, the Pt_{10} model enables the incorporation of multiple co-adsorbed CO species, thereby providing a more realistic description of surface environments under high CO coverage. Free-energy profiles were calculated by pre-adsorbing one, two, and three CO molecules on the Pt_{10} cluster, corresponding to progressively increasing degrees of local CO accumulation (Fig. 6b).

The calculations reveal a pronounced dependence of the RWGS energetics on surface CO coverage. At low CO coverage, H_2 adsorption and dissociation are thermodynamically favorable. However, as the number of pre-adsorbed CO molecules increases from 1 to 3, the resulting depletion of available Pt active sites (site blocking) dramatically weakens the thermodynamic driving force for hydrogen activation, shifting the free energy from − 2.23 eV to − 0.65 eV. Because kinetic isotope effect measurements identified H_2 dissociation as the kinetically relevant step of the RWGS reaction, suppression of H_2 activation is expected to directly impair the overall catalytic activity. Furthermore, this suppressed H_2 activation exerts a cascading inhibitory effect on the entire redox cycle. The hampered supply of highly mobile atomic hydrogen severely slows down the reduction of the oxidized support, thereby impeding the regeneration of critical oxygen vacancies. As a direct result, the barrier for CO_2 dissociation at these vacancy sites surges from 1.10 eV (with 1 pre-adsorbed CO) to 2.07 eV and 2.59 eV (with 2 and 3 pre-adsorbed CO molecules, respectively). In addition, the subsequent H_2O-formation steps ($2^*H + {}^*O \rightarrow {}^*OH + {}^*H$ and $^*H + {}^*OH \rightarrow H_2O + 2^*$) also become progressively less favorable, with the corresponding barriers increasing from 1.90 and 0.77 eV at low CO coverage to 2.44 and 1.33 eV at higher CO coverage. Therefore, elevated CO surface populations exert a broad inhibitory effect across multiple elementary steps of the RWGS reaction.

Collectively, these calculations demonstrate that excessive CO accumulation exerts a broad inhibitory effect on the RWGS reaction by simultaneously suppressing hydrogen activation, impeding oxygen-vacancy regeneration, and increasing the energetic demands of multiple elementary reaction steps. These results provide a quantitative explanation for the experimentally observed activity enhancement under illumination and highlight the critical importance of dynamically regulating steady-state CO coverage during RWGS catalysis.

3 Conclusion

In summary, this work demonstrates that regulating steady-state adsorbate coverage under reaction conditions is a critical yet often overlooked factor governing heterogeneous catalytic performance. Taking the RWGS reaction as a representative example, the strong adsorption of CO on Pt under conventional thermocatalytic conditions can lead to substantial site blocking, thereby suppressing H_2 dissociation and progressively hindering the catalytic cycle. To address this challenge, we designed a Pt-MoO_{3-x} catalyst and demonstrated that light irradiation can dynamically regulate surface CO coverage during the reaction, thereby mitigating catalyst poisoning under operating conditions. In situ XPS measurements reveal illumination-induced electron enrichment at Pt sites, consistent with charge redistribution across the Pt–O–Mo interface, while in situ spectroscopic measurements demonstrate a reduction in steady-state CO coverage. Theoretical calculations further elucidate that the modified electronic structure of Pt alters the Pt–CO interaction, providing an electronic-structure basis for the experimentally observed regulation of surface CO coverage. As a result, compared with thermocatalysis at an identical catalyst temperature, the Pt- MoO_{3-x} catalyst exhibits substantially enhanced RWGS activity under mild illumination conditions, indicating a contribution beyond purely photothermal heating.

More broadly, this work establishes light-mediated regulation of adsorbate coverage as an effective strategy for mitigating product-induced catalyst poisoning. Beyond the RWGS reaction, the concept of dynamically controlling surface intermediates through electronic-structure modulation may provide new opportunities for improving the activity and stability of a wide range of heterogeneous catalytic systems.

Declarations

Acknowledgements

This work was financially supported by the Scientific Research Innovation Capability Support Project for Young Faculty (SRICSPYF-BS2025054), National Natural Science Foundation of China (22572104, U23A20136), the Self-Developed Instrument Project of Shandong University (ZY20240302), and the Outstanding Young Scholars Projects of Shandong University.

References

1. aA. J. Martín, S. Mitchell, C. Mondelli, S. Jaydev, J. Pérez-Ramírez, *Nature Catalysis* **2022**, *5*, 854-866; bD. Kiani, I. E. Wachs, *ACS Catalysis* **2024**, *14*, 16770-16784.
2. I. Omae, *Coordination Chemistry Reviews* **2012**, *256*, 1384-1405.
3. E. Pahija, C. Panaritis, S. Gusarov, J. Shadbahr, F. Bensebaa, G. Patience, D. C. Boffito, *ACS Catalysis* **2022**, *12*, 6887-6905.
4. M. Ahmadi Khoshooei, X. Wang, G. Vitale, F. Formalik, K. O. Kirlikovali, R. Q. Snurr, P. Pereira-Almao, O. K. Farha, *Science* **2024**, *384*, 540-546.
5. aW. Li, J. Gan, Y. Liu, Y. Zou, S. Zhang, Y. Qu, *Angewandte Chemie International Edition* **2023**, *62*, e202305661; bH.-X. Liu, J.-Y. Li, X. Qin, C. Ma, W.-W. Wang, K. Xu, H. Yan, D. Xiao, C.-J. Jia, Q. Fu, D. Ma, *Nature Communications* **2022**, *13*, 5800; cX. Hu, D. Xu, J. Jiang, *Angewandte Chemie International Edition* **2025**, *64*, e202419103; dW. Bi, J. Wang, R. Zhang, Q. Ge, X. Zhu, *ACS Catalysis* **2024**, *14*, 11205-11217.
6. W. Miao, R. Hao, L. Gan, W. Xu, Z. Wang, W. Lin, H. Liu, Y. Lyu, Q. Li, J. Xi, A. Nie, J. Wu, H. Wang, *Journal of Energy Chemistry* **2025**, *101*, 733-743.
7. D. Long, X. Ping, J. Ni, F. Chen, S. Chen, Z. Wei, L. Guo, J. Zheng, *Chemical Communications* **2023**, *59*, 13583-13586.
8. J. P. Perdew, K. Burke, M. Ernzerhof, *Physical Review Letters* **1996**, *77*, 3865-3868.
9. S. Li, X. Liu, J. Ma, F. Xu, Y. Lyu, S. Perathoner, G. Centi, Y. Liu, *ACS Catalysis* **2025**, *15*, 3475-3486.
10. C. D. Lindstrom, X. Y. Zhu, *Chem. Rev.* **2006**, *106*, 4281-4300.
11. aD. Menzel, R. Gomer, *The Journal of Chemical Physics* **1964**, *41*, 3311-3328; bM. Bonn, S. Funk, C. Hess, D. N. Denzler, C. Stampfl, M. Scheffler, M. Wolf, G. Ertl, *Science* **1999**, *285*, 1042-1045; cI. Barraza Alvarez, T. Le, H. Hosseini, S. Samira, A. Beck, J. Marlowe, M. M. Montemore, B. Wang, P. Christopher, *Journal of the American Chemical Society* **2024**, *146*, 12431-12443.

12. D. Lichtman, *Surface Science* **1979**, *90*, 579-587.
13. X. Yu, N. S. Genz, R. G. Mendes, X. Ye, F. Meirer, M. Nachtegaal, M. Monai, B. M. Weckhuysen, *Nature Communications* **2024**, *15*, 6494.
14. Z.-X. Sun, C. Zhou, Z. Chen, Y. Zeng, T. Sun, X. Dong, L. Yang, X. Wang, Q. Wu, H. Huang, L. He, Z. Hu, *Angewandte Chemie International Edition* **2025**, *64*, e202508090.
15. H. Cheng, T. Kamegawa, K. Mori, H. Yamashita, *Angewandte Chemie International Edition* **2014**, *53*, 2910-2914.
16. H. Wang, F. Wang, S. Zhang, J. Shen, X. Zhu, Y. Cui, P. Li, C. Lin, X. Li, Q. Xiao, W. Luo, *Advanced Materials* **2024**, *36*, 2400764.
17. aX. Han, L. Jiang, Z. Zhang, K. Liu, M. Bian, Z. Yuan, Y. Li, C. Rao, X. Yang, Y. Zhang, *Environmental Science & Technology* **2025**, *59*, 12364-12377; bJ. Liu, W. Liu, Z. Li, J. Wang, R. Fan, C. Liu, B. Gao, Z. Zou, Z. Li, *ACS Catalysis* **2025**, *15*, 10470-10479; cM. Zhou, J. Li, L. Qu, W. Zhang, T. Liu, Y. Liu, F. Wang, Y. Ding, Z. Zhou, Y. Pi, Y. Chen, S. Lee, G. Wang, X. Liao, Y. Zhao, L. Mai, Z. Wang, *Applied Catalysis B: Environment and Energy* **2026**, *383*, 126058.
18. aF. C. Meunier, T. Elgayyar, K. Dembélé, H. Kaper, in *Catalysts, Vol. 12*, **2022**, p. 532; bA. Bourane, O. Dulaurent, D. Bianchi, *Journal of Catalysis* **2000**, *196*, 115-125.
19. P. Hollins, *Surface Science Reports* **1992**, *16*, 51-94.
20. aX. Su, X. Yang, B. Zhao, Y. Huang, *Journal of Energy Chemistry* **2017**, *26*, 854-867; bH.-X. Liu, S.-Q. Li, W.-W. Wang, W.-Z. Yu, W.-J. Zhang, C. Ma, C.-J. Jia, *Nature Communications* **2022**, *13*, 867.
21. aX. Chen, X. Su, B. Liang, X. Yang, X. Ren, H. Duan, Y. Huang, T. Zhang, *Journal of Energy Chemistry* **2016**, *25*, 1051-1057; bH.-X. Liu, W.-W. Wang, X.-P. Fu, J.-C. Liu, C.-J. Jia, *Nature Communications* **2024**, *15*, 9126.
22. aP. Jin, P. Guo, N. Luo, H. Zhang, C. Ni, R. Chen, W. Liu, R. Li, J. Xiao, G. Wang, F. Zhang, P. Fornasiero, F. Wang, *Science* **2025**, *389*, 1037-1042; bH. Liang, B. Zhang, P. Gao, X. Yu, X. Liu, X. Yang, H. Wu, L. Zhai, S. Zhao, G. Wang, A. P. van Bavel, Y. Qin, *Chem Catalysis* **2022**, *2*, 610-621.

Figures

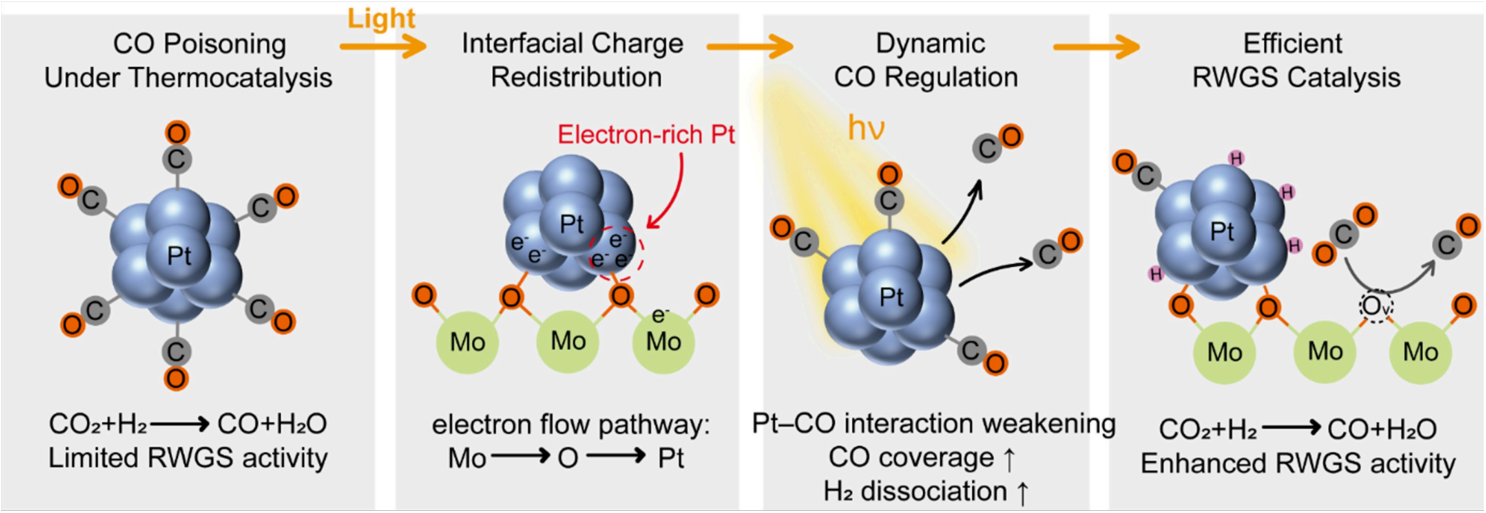


Figure 1

Schematic illustration of the illumination-induced dynamic regulation of steady-state CO surface coverage over electron-rich Pt–MoO_{3-x} catalysts for the RWGS reaction. Under thermocatalytic conditions, strongly adsorbed CO accumulates on Pt surfaces, resulting in catalyst poisoning and limited RWGS activity. Upon illumination, interfacial charge redistribution across the Pt–O–Mo interface enriches the electron density of Pt sites, weakens Pt–CO interactions, and promotes CO desorption, thereby dynamically decreasing the steady-state CO coverage. The released Pt active sites facilitate H_2 dissociation and oxygen-vacancy regeneration, ultimately leading to enhanced RWGS activity.

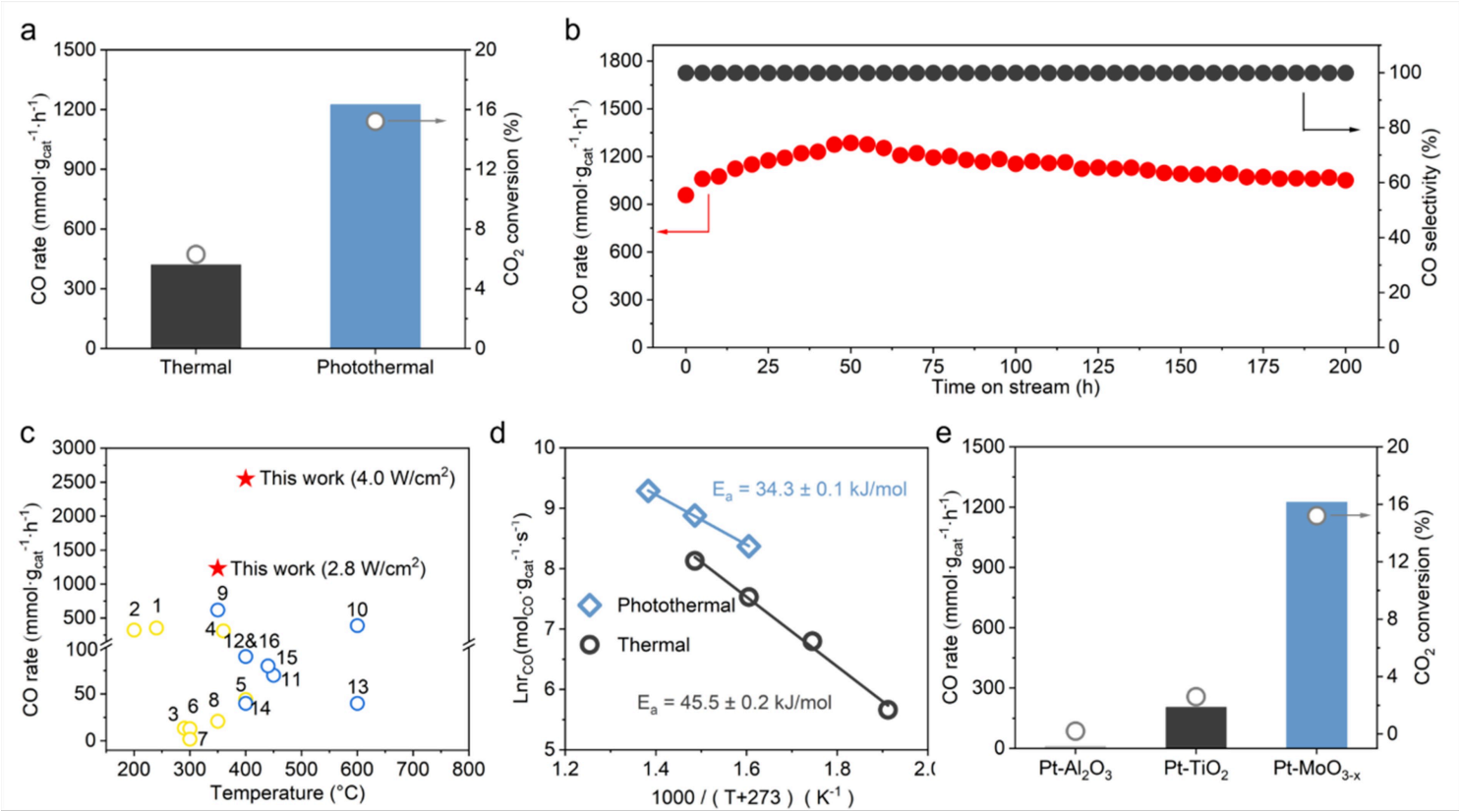


Figure 2

Catalytic performance of Pt-MoO_{3-x} for the low-temperature RWGS reaction. (a) CO production rates under dark and full-spectrum illumination (2.8 W cm^{-2}) at identical catalyst bed temperatures (350 °C). (b) Long-term stability test of the Pt-MoO_{3-x} catalyst under light irradiation. (c) Comparison of catalytic performance with reported thermal (blue circle) and photo-assisted (yellow circle) catalysts as a function of reaction temperature. (d) Arrhenius plots and the corresponding apparent activation energies (E_a) under dark and light conditions. (e) CO production rates of Pt loaded on different oxide supports under identical illumination conditions.

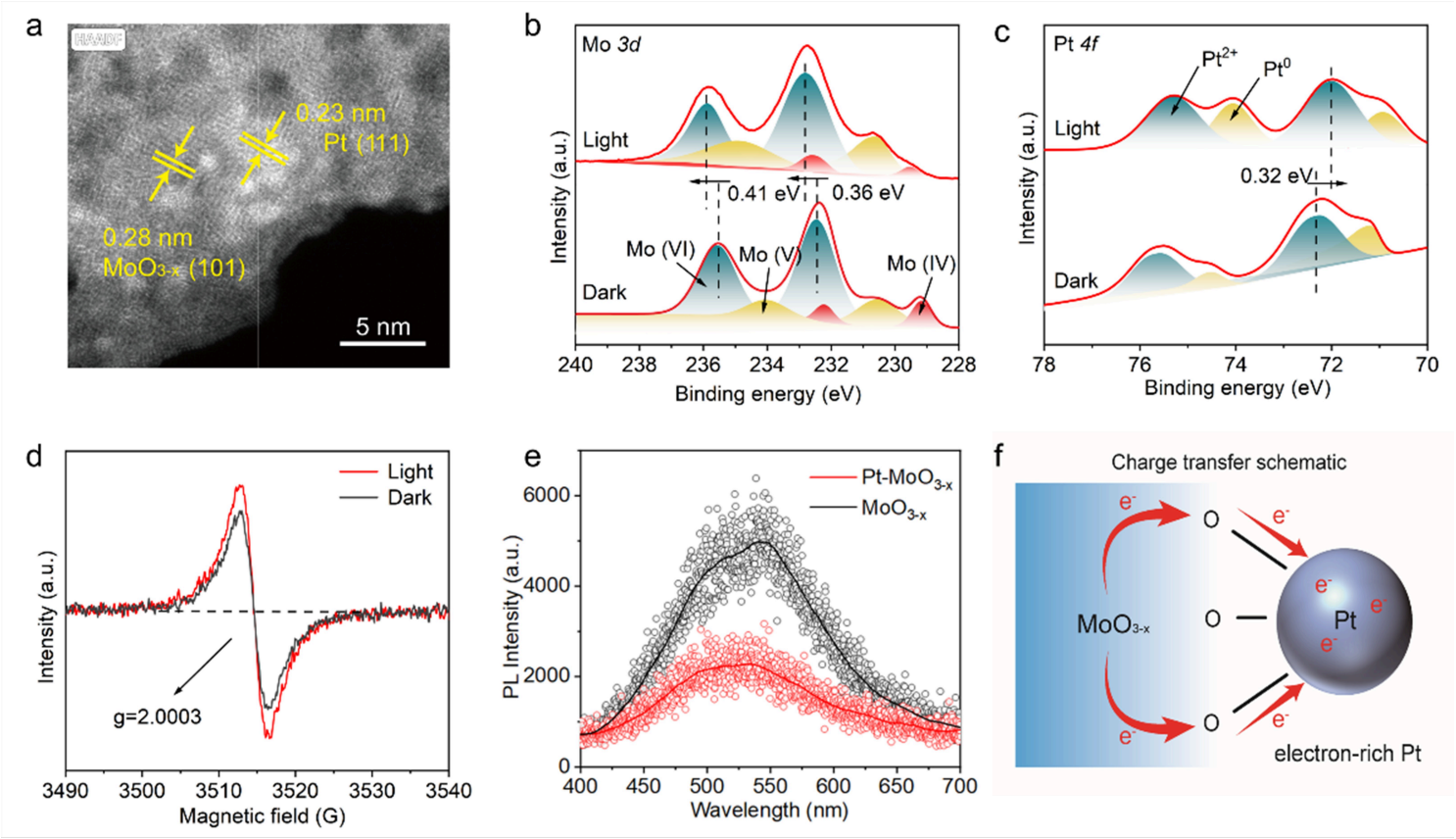


Figure 3

Structural and interfacial electronic characterizations of the Pt-MoO_{3-x} catalyst. (a) HRTEM of the Pt-MoO_{3-x} interface. In situ XPS spectra of (b) Mo *3d* and (c) Pt *4f* for Pt-MoO_{3-x} under dark and illuminated conditions. (d) EPR spectra confirming the presence of oxygen vacancies in MoO_{3-x}. (e) PL spectra of Pt-MoO_{3-x} and MoO_{3-x}. (f) Schematic illustration of interfacial charge transfer.

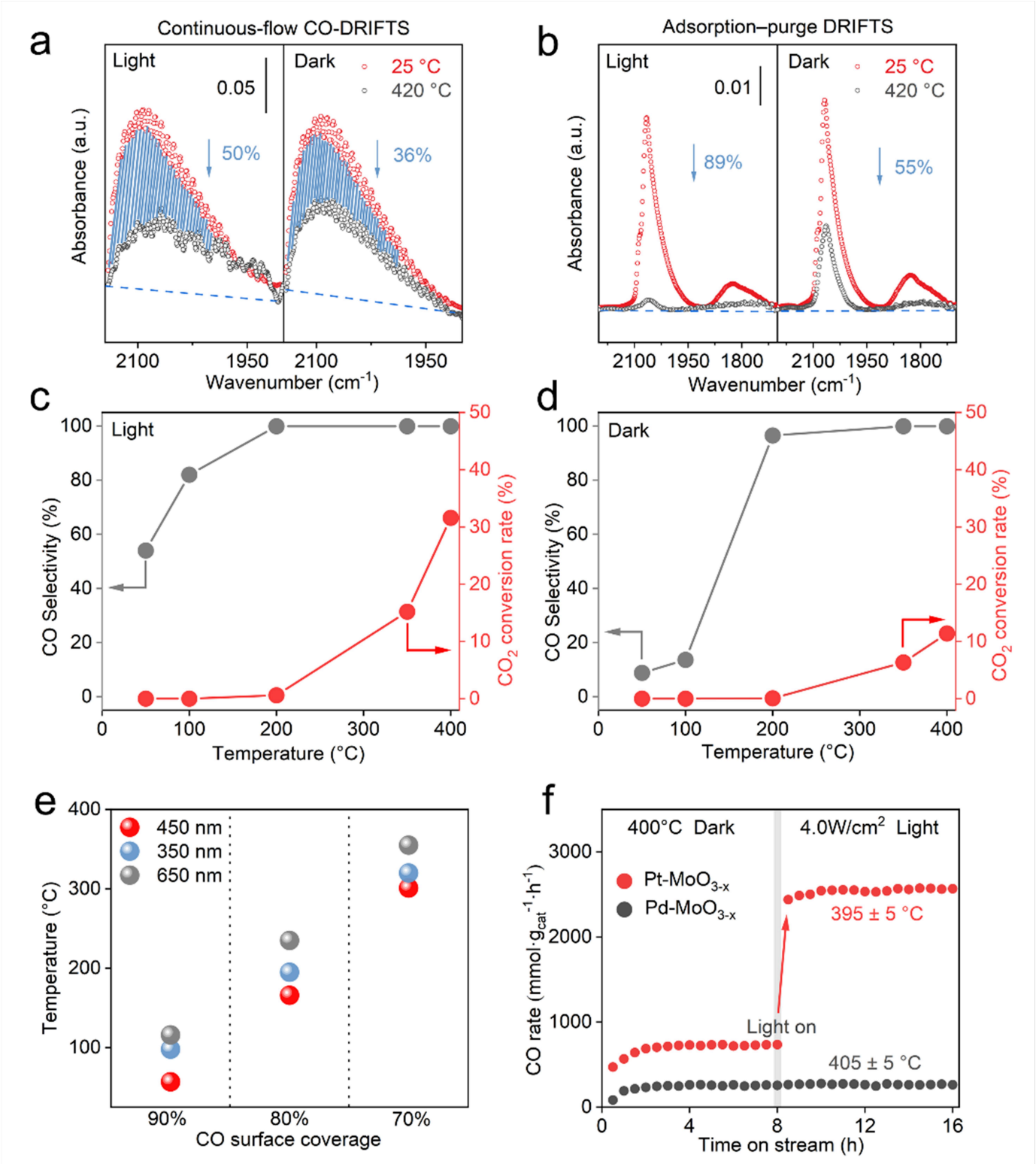


Figure 4

Spectroscopic and catalytic evidence for the dynamic light regulation of surface CO coverage. (a) Continuous-flow CO-DRIFTS spectra of Pt-MoO_{3-x} under light irradiation and dark conditions. (b) Adsorption–purge DRIFTS spectra of Pt-MoO_{3-x} under light irradiation and dark conditions. (c, d) CO selectivity and CO_2 conversion as a function of temperature under (c) light and (d) thermal conditions.

(e) Wavelength-dependent CO desorption behavior of Pt-MoO_{3-x}. (f) Light on-off switching experiment comparing Pt-MoO_{3-x} and Pd-MoO_{3-x}.

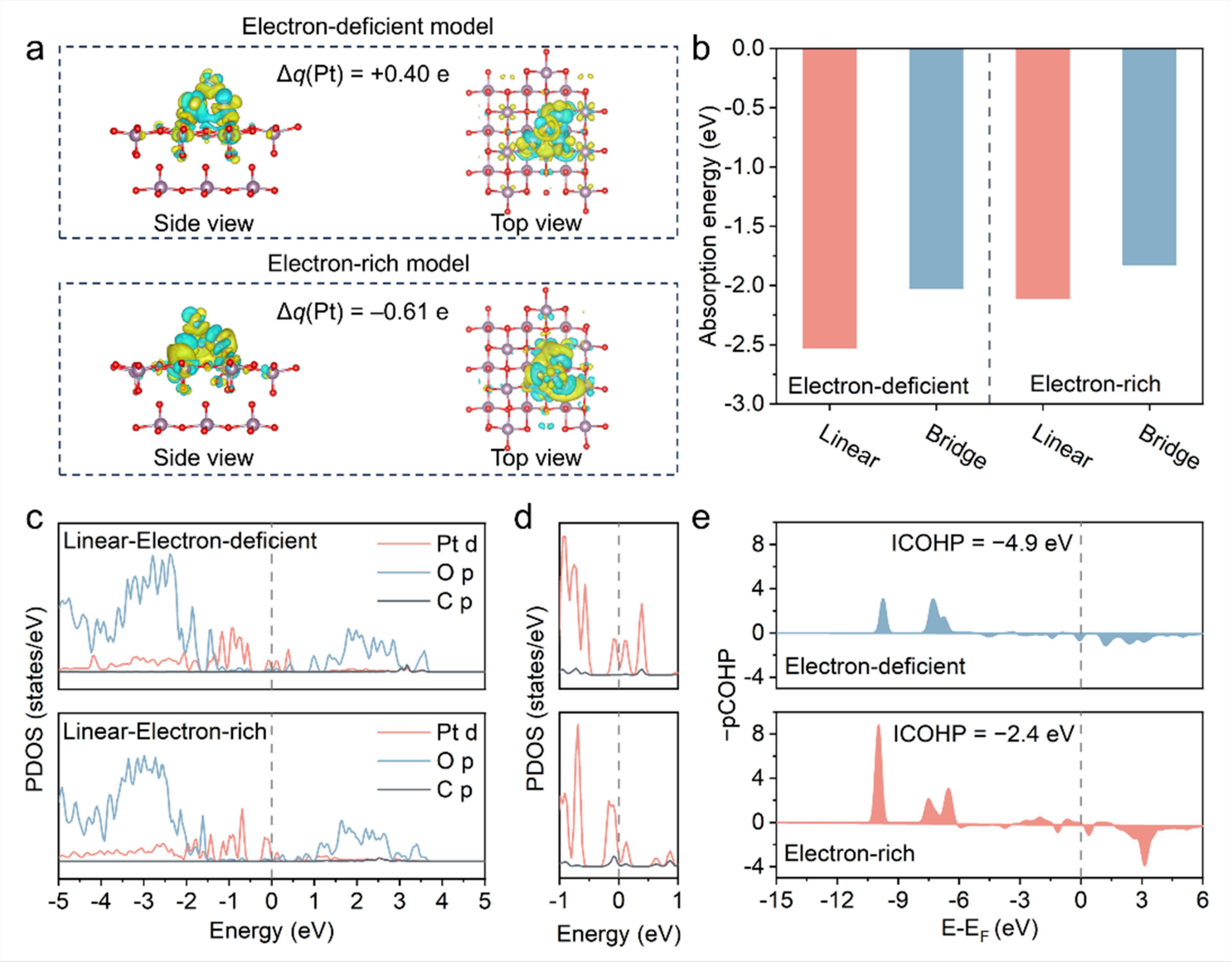


Figure 5

DFT analysis of the influence of Pt electronic structure on CO adsorption. (a) Three-dimensional charge density difference distributions and net charge transfer for Pt_4 clusters supported on pristine MoO_3 and oxygen-deficient MoO_{3-x} surfaces. Yellow and cyan regions represent electron accumulation and depletion, respectively. (b) Calculated adsorption energies of linear and bridge-bonded CO species on electron-deficient model and electron-rich model. (c) PDOS of linearly adsorbed CO on the two models. (d) Enlarged view of the PDOS near the Fermi level. (e) −pCOHP analysis and ICOHP values of the Pt–C interaction for linearly adsorbed CO.

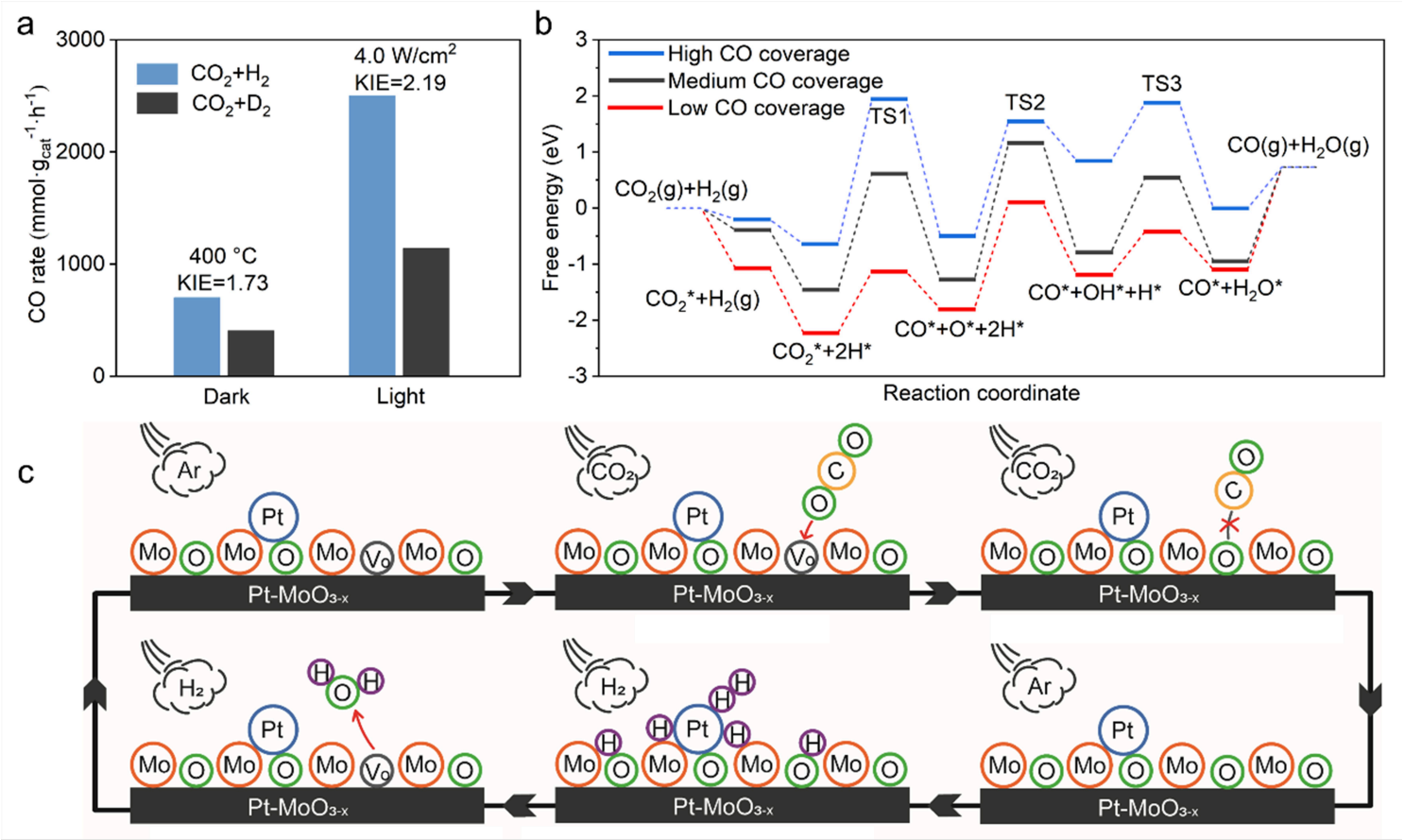


Figure 6

Mechanistic investigation of the RWGS reaction over Pt-MoO_{3-x}. (a) Kinetic isotope effect values for H_2/D_2 substitution under dark and light conditions. (b) DFT-calculated free energy profiles for the RWGS reaction over Pt-MoO_{3-x} at varying CO surface coverages. (c) Proposed RWGS reaction mechanism on Pt-MoO_{3-x}.

Supplementary Files

This is a list of supplementary files associated with this preprint. Click to download.

- SupportingInformation.docx